# Dynamic testing of shock absorbers under non-sinusoidal conditions

**D Kowalski**[1], **M D Rao**[1]*, **J Blough**[2] and **S Gruenberg**[2]
[1]Michigan Technological University, Houghton, Michigan, USA
[2]Keweenaw Research Center, Michigan Technological University, Michigan, USA

**Abstract:** This paper deals with the dynamic characterization of an automotive shock absorber, the continuation of an earlier work [**1**]. The objective of this ongoing research is to develop a testing and analysis methodology for obtaining dynamic properties of automotive shock absorbers for use in CAE-NVH low-to-mid-frequency chassis models. Stepped sine sweep excitation is currently used in industry to obtain shock absorber parameters along with their frequency and amplitude dependence. Sine-on-sine testing, which involves excitation using two different sine waves, has been done in this study to understand the effects of the presence of multiple sine waves on the estimated dynamic properties. In an effort to obtain all frequency dependent parameters simultaneously, different types of broadband random excitation have also been studied. Results are compared with stepped sine sweep tests. Additionally, actual road data measured on different road profiles have been used as input excitation to obtain the shock absorber parameters for broad frequency bands under realistic amplitude and frequency conditions. These results are compared with both simulated random excitation and stepped sine sweep test results.

**Keywords:** shock absorbers, dynamic properties, damping, sine-on-sine excitation, struts

## NOTATION

| | |
|---|---|
| $a$ | acceleration |
| $C$ | damping parameter |
| $f$ | frequency (cycles/s) |
| $F$ | output force |
| FRF | frequency response function |
| $K$ | stiffness parameter |
| $K^*$ | magnitude of complex stiffness (also called dynamic stiffness) |
| $v$ | velocity |
| $x$ | displacement |
| $\Phi$ | phase angle between input displacement and output force (rad) |
| $\omega$ | frequency (rad/s) |

## 1 INTRODUCTION

The shock absorber is one of the most important elements in a vehicle suspension system. It is also one of the most non-linear and complex elements to model. Parametric and non-parametric models exist for modelling shock absorbers. A non-parametric model based on a restoring force surface mapping has been developed [**2**–**4**]. The model considers the force to be a function of displacement and velocity. Although this model is more applicable to a single frequency excitation, it serves as a useful tool for identifying the non-linearities in the system.

A comprehensive physical model was developed by Lang [**5**] and later condensed and validated by Morman [**6**]. Lang's model has more than 80 parameters, is computationally complex and is not suitable for comprehensive vehicle simulation studies. Morman's model has been shown to be useful for studying the effects of design changes for a particular shock absorber. Reybrouck [**7**] has developed a physical model, which has 14 parameters, valid for frequencies of up to 20 Hz, and hence has limited appeal for the analysis of shock absorbers for high-frequency NVH applications. The current industry standard method of characterizing the dynamic properties of shock absorbers for computer simulation models involves testing at discrete frequencies, displacements and preloads using a hydraulic test machine. The stiffness, $K$, and damping coefficient, $C$, are extracted

*The MS was received on 24 July 2001 and was accepted after revision for publication on 16 January 2002.*
* *Corresponding author: Michigan Technological University, 1400 Townsend Drive, Houghton, MI 49931, USA.*

by fitting a linear model of the form $F(\omega) = Kx(\omega) + Cv(\omega)$ to the measured input displacement, $x$, velocity $v$, and output force, $F$. The excitation technique is a pure sine excitation at the desired frequency and amplitude. These harmonic excitations are then swept through all desired frequencies and amplitudes.

The goal of this study was to determine if the current excitation and analysis techniques are applicable when more than one frequency is present in the input excitation. The first task included standardizing the test procedure. This is done because shock absorber parameters vary with temperature and nominal length. Sine-on-sine testing and different types of broadband random excitations have been utilized. Results are compared with stepped sine sweep tests. Additionally, actual road data have been used as input excitation to obtain the shock absorber parameters under realistic amplitude and frequency conditions. Details of these are presented in the following sections.

## 2 TEST PROCEDURE

All of the testing for this project was done using the MTS 831 elastomer characterization machine located at the Keweenaw Research Center of Michigan Technological University. A picture of a shock absorber in the test fixture is shown in Fig. 1. The hardware used to control the MTS 831 was TestStar II. In conjunction with TestStar II, TestWare-SX software was used to organize a test matrix and also to monitor and record the desired parameters throughout the test. TestWare-SX, however, is only capable of producing pure sine excitations. Therefore, component RPCIII (cRPC) software was used to excite the test specimen with user-defined excitation. The cRPC has the ability to generate pure sine waves, multiple sine waves, shaped random excitations or any arbitrary time domain excitation.

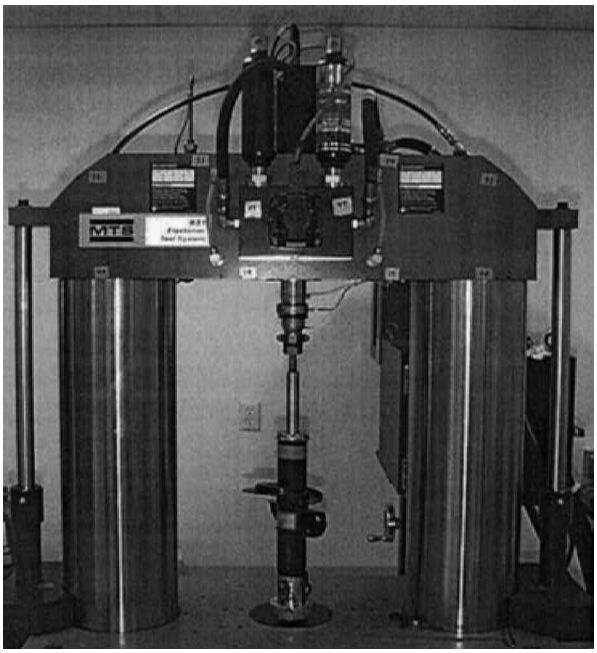


**Fig. 1** MTS 831 machine with shock absorber installed

### 2.1 Analysis

TestWare-SX creates a frequency response function (FRF) between the output force and the input displacement. The magnitude of the FRF is the dynamic stiffness, $K^*$, and the phase of the FRF is related to the damping coefficient, $C$. The stiffness parameter, $K$, is the real part of the FRF, $K = K^* \cos(\Phi)$, and the damping coefficient is the imaginary part of the FRF divided by the frequency $\omega$, $C = (K^*/\omega) \sin(\Phi)$. This analysis procedure can be extended to all frequencies by realizing that $K^*$ and $\Phi$ are simply the magnitude and phase of the FRF between the output force and input displacement. The stiffness term in a typical pressurized shock absorber refers to the stiffness of the gas/air in the tube as well as the stiffness of the seals and gaskets.

### 2.2 Pure sine sweep tests

In order to understand the effects of multiple sine waves on $K$ and $C$, a baseline for the shock absorber parameters was first established. The baseline consisted of testing with pure sine waves with zero-to-peak amplitudes of 0.1, 0.25, 0.35 and 0.5 mm. The frequencies chosen for the pure sine waves were 5, 10, 20, 30, 40, 80, 120 and 140 Hz. The maximum frequency of the anti-alias filter on the cRPC boards was 160 Hz; therefore, the upper frequency limit was below this to eliminate possible aliasing effects. The force transducer established the lower frequency limit on the MTS 831, which was determined to be approximately 4 Hz. The results of the baseline testing are shown in Fig. 2. It can be seen clearly that stiffness increases as a function of frequency. However, no clear trend is evident for stiffness as a function of displacement amplitude. It is also seen that the damping estimates decrease significantly as a function of frequency and amplitude for frequencies below 80 Hz. Above 80 Hz, the damping does not appear to change with an increase in frequency.

## 3 SINE-ON-SINE EXCITATION

Having established the baseline, this study was focused on how the stiffness and damping parameters change when two frequencies are present simultaneously. The motivation for this inquiry is that, in practice, shock absorbers experience multiple frequencies simultaneously.

 

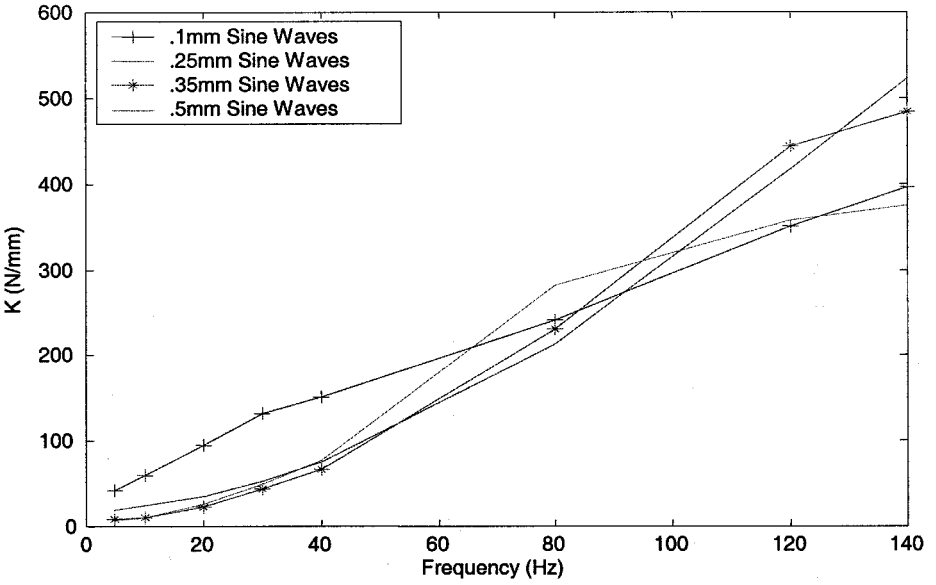


(a)

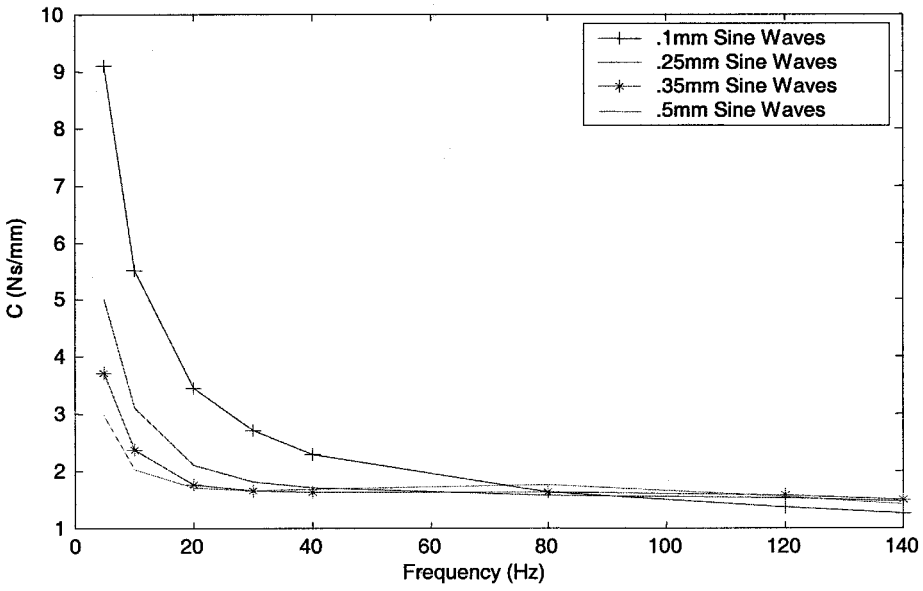


(b)

**Fig. 2** Damping and stiffness versus frequency from sine sweep testing

Before the shock can be studied with many frequency inputs, the effects must first be understood for two frequencies. The hypothesis is that, when a higher-frequency wave is superimposed on a lower-frequency wave, the lower-frequency wave breaks the static friction (stiction) of the shock, resulting in a lower force requirement to move the shock at the higher frequency. Therefore, a lower stiffness estimate would be obtained at the higher frequency. An example of a sine-on-sine input is shown in Fig. 3. It can be seen that the lower-frequency, higher-amplitude wave appears as if it is carrying the higher-frequency, lower-amplitude wave. For this reason, the lower-frequency wave is referred to as the carrier wave and the higher-frequency wave is referred to as the rider wave.

In order to understand this sine-on-sine excitation, a test matrix was determined as follows. The frequencies of 5, 10, 20 and 30 Hz are the carrier wave frequencies. These frequencies were held at a constant amplitude of 0.5 mm. The frequencies of 40, 80, 120 and 140 Hz are the rider frequencies. These frequencies will be added to the carrier wave frequencies at amplitudes of 0.1, 0.25, 0.35 and 0.5 mm. In summary, this results in four different rider frequencies at four distinct amplitudes being

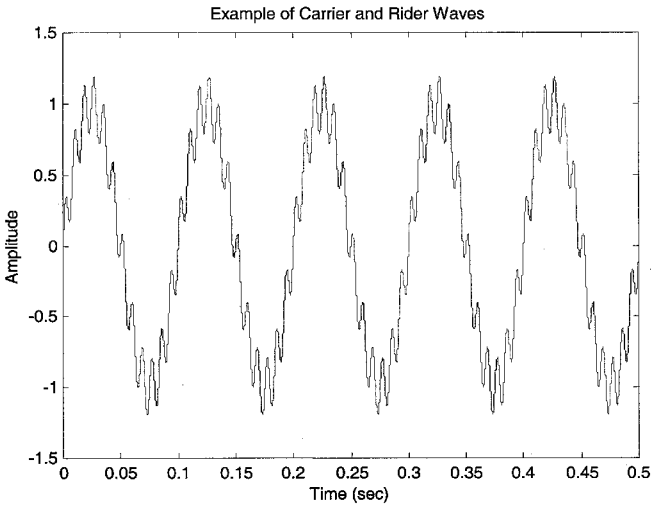


**Fig. 3** Example of a combined carrier and rider wave

added to each of the four different carrier wave frequencies. This results in a total of 64 different test conditions.

### 3.1 Stiffness estimates of rider waves

Figures 4a to d show the effects that the carrier wave frequencies have on the rider wave stiffness estimates. Each graph is for a rider wave amplitude and plots the rider wave stiffness estimates versus frequency. Each series on these plots is for a different carrier wave frequency. Also plotted are the values of stiffness, at the appropriate amplitude, for the rider waves as pure sine inputs. When the rider amplitude is 0.1 mm, the variance of the estimations is greatest. This is believed to be due to the fact that 0.1 mm amplitudes are approaching the noise floor of the measurement system. At all of the higher-amplitude rider waves, the variance is less. The stiffness estimates at the rider wave frequencies seem to be independent of both the frequency of the carrier wave and the existence of a carrier wave. In conclusion, the existence of a carrier wave has little effect on the estimates of stiffness at the rider wave frequencies.

### 3.2 Damping estimates of rider waves

Figures 4e to h show these results. The damping estimates below 100 Hz, for the rider frequencies, do not approximate the pure sine estimates as closely as the stiffness estimates. However, above 100 Hz, the rider wave damping estimates obtained with sine-on-sine input are approximately the same as the estimates obtained using pure sine input excitation. Another interesting result shown in these figures is that the damping estimates increase, relative to the pure sine estimates, as the rider wave amplitude increases. Hence, at the lower-amplitude rider waves the pure sine test gives the highest estimate, whereas at the higher-amplitude rider waves they yield the lowest estimates.

### 3.3 Stiffness estimates of carrier waves

Figures 4i to l plot the results of stiffness estimates for the carrier waves. These plots are shown in the same manner as the rider wave results. Each graph is for one rider wave amplitude. Each series on these graphs is for a single rider wave frequency. It can be seen that the stiffness estimates for the carrier waves are affected by the presence of a rider wave. With the exceptions of carrier waves of 20 and 30 Hz, for a rider wave frequency of 40 Hz and amplitude of 0.5 mm, all of the carrier wave stiffness estimates are below the pure sine stiffness estimates. These graphs also show that the stiffness estimates for the carrier waves decrease as the rider frequency is increased. This is clearly evident in Fig. 4l where the amplitudes of the rider and carrier waves are equal. Following the 140 Hz rider wave through all the amplitudes shows that the carrier wave stiffness estimates decrease as the rider amplitude increases. This trend is clearly evident when the 140 Hz rider amplitude is equal to the carrier amplitudes, because the stiffness of the carrier waves approaches zero.

### 3.4 Damping estimates of carrier waves

Figures 4m to p show the damping estimates for the carrier waves as a function of frequency. When comparing the damping results of the carrier waves with the damping results of the rider waves, the carrier wave estimates are affected more than the rider estimates. The estimates are scattered with no clear trend emerging.

### 3.5 Conclusions from sine-on-sine testing

The overall outcome of adding two sine waves together is interesting and the results reveal some trends. The estimates of dynamic properties at higher-frequency waves are far less affected by the presence of the lower-frequency wave than the opposite. This is evident from the stiffness estimates for the higher-frequency waves being much closer to the values obtained with pure sine inputs. It is also demonstrated by the damping estimates, which are much closer to the pure sine values for the higher-frequency waves. In general, the higher-frequency wave dominates the parameter estimates for the shock absorber. This is demonstrated by the highest-frequency rider wave, of 140 Hz, at the largest amplitude of 0.5 mm. When this wave was added to the lower-frequency carrier waves, the parameters estimated at 140 Hz were almost the same as the 140 Hz pure sine wave. On the other hand, the parameters estimated at the lower carrier frequencies tend towards zero.

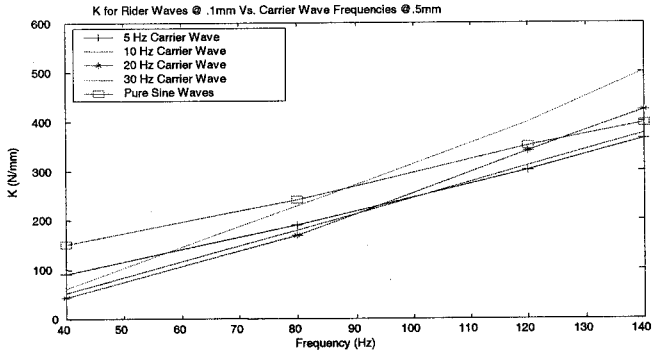


(a)

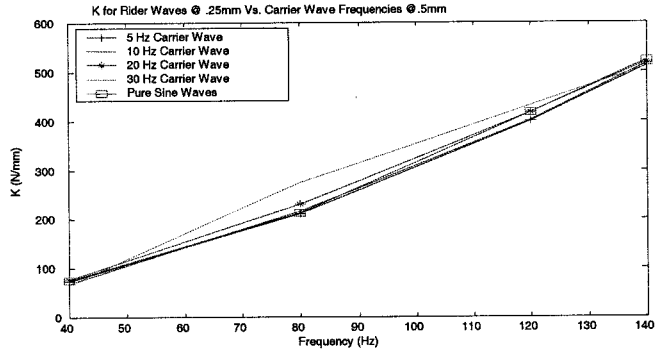


(b)

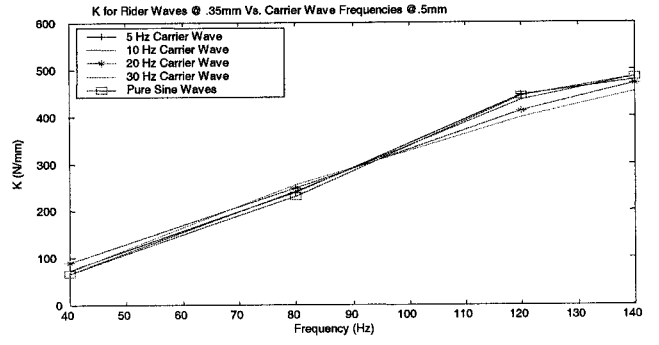


(c)

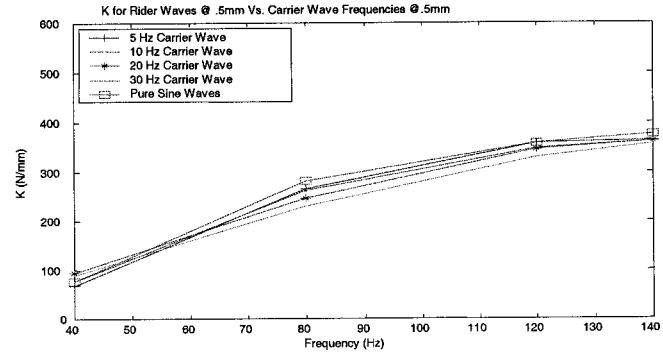


(d)

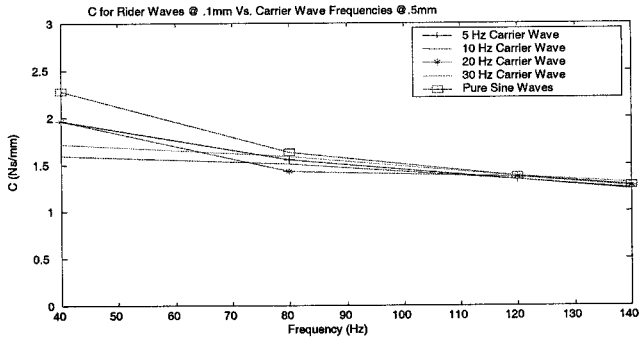


(e)

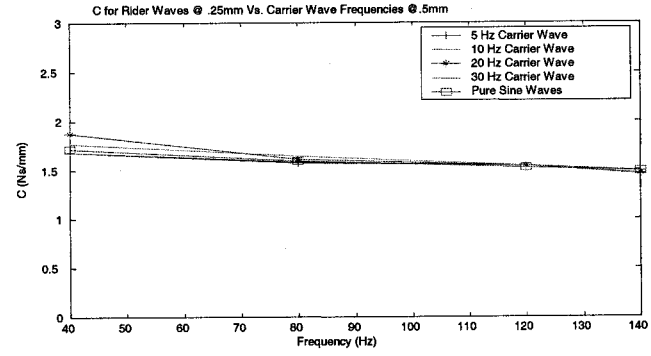


(f)

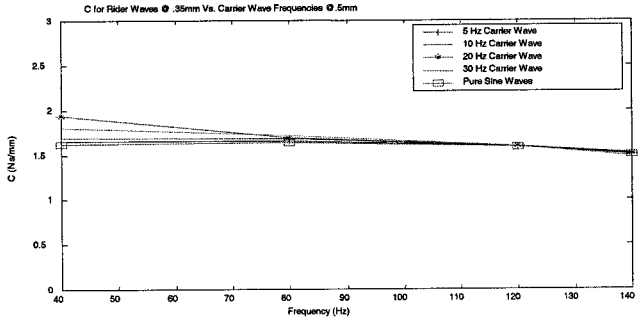


(g)

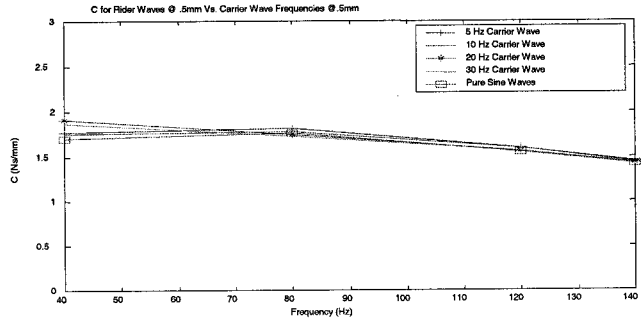


(h)

**Fig. 4** (continued over.)

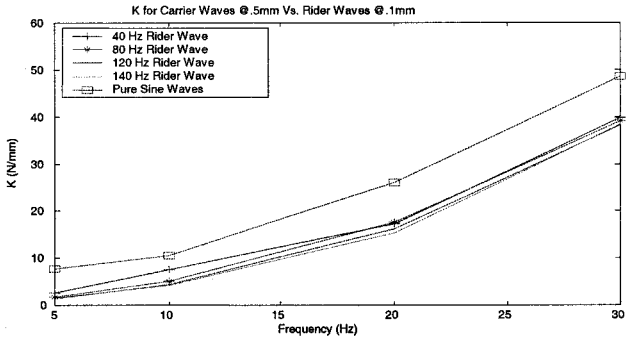


(i)

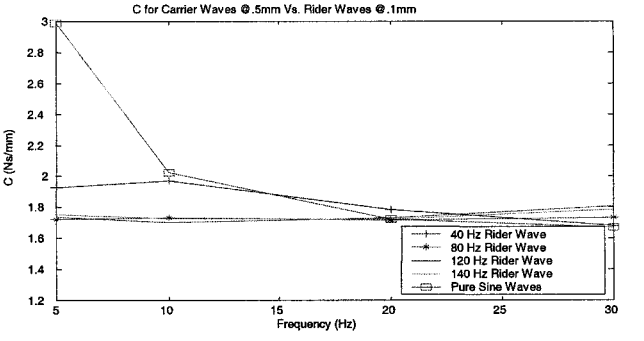


(m)

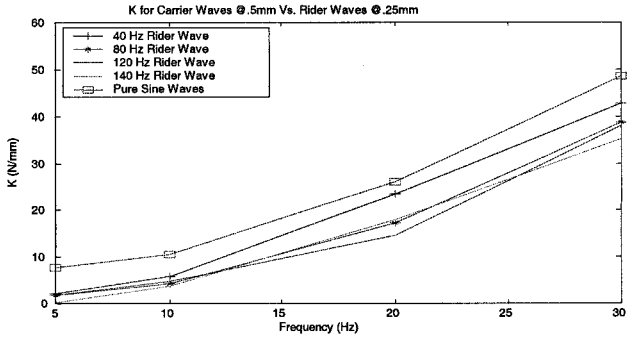


(j)

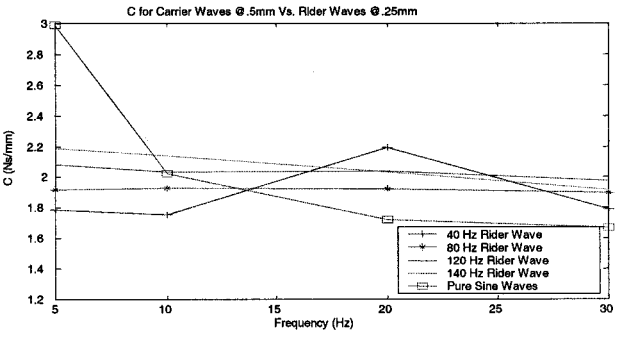


(n)

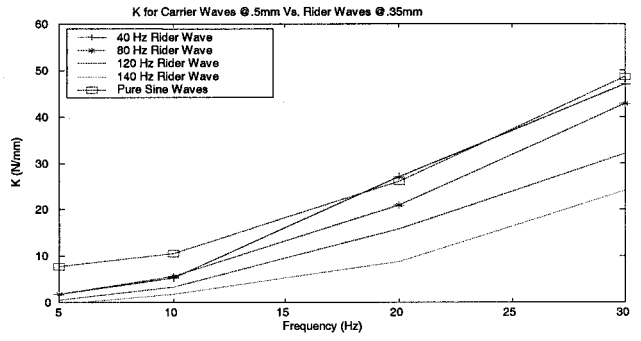


(k)

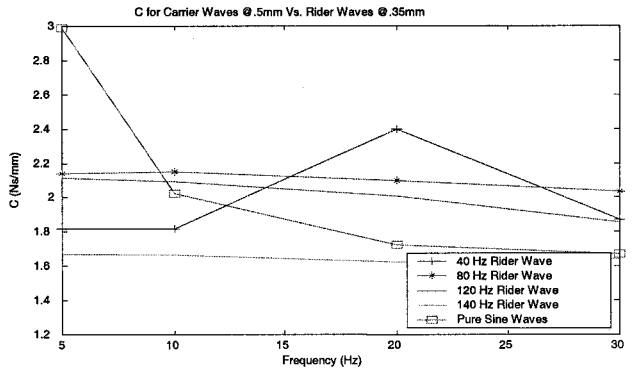


(o)

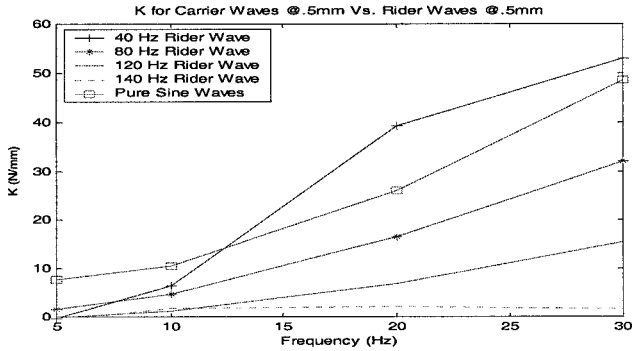


(l)

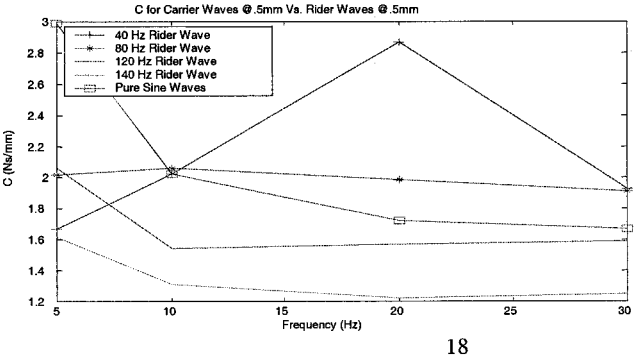


18

(p)

**Fig. 4** Effects of carrier wave frequency on (a to d) rider wave stiffness and (e to h) rider wave damping, and effects of amplitude of rider wave on (i to l) carrier wave stiffness and (m to p) carrier wave damping

 

## 4 MULTIPLE-FREQUENCY INPUT EXCITATION

Having examined the sine-on-sine input excitation, the next step was to determine the effects when all the frequencies of interest are present in the input excitation. It was decided to use random signals with the same overall amplitudes as the previous sine waves. For this study, the peak-to-peak values of the random excitation was 1 mm. This value was chosen because results of this can be compared with previous tests with pure sines having the same peak-to-peak values. Also, it yielded the best signal-to-noise ratio among the available sine input amplitudes. Random input signals were generated in three different ways for this study. The first random signal generated has a constant amplitude for all frequencies. The second type of random signal generated weights the amplitudes at $1/f^1$. The final type of random signal weights the amplitudes at $1/f^2$. It is important to remember that the peak-to-peak values of all three of these random signals is kept at 1 mm. This does mean, however, that the amplitude at a given frequency changes from drive file to drive file. The power spectral densities of the input displacement and the output force of these three signals can be seen in Fig. 5. The analysis to obtain stiffness and damping is done spectral line by spectral line. The results of stiffness and damping estimates are shown in Fig. 6. Examining the damping estimate first, it is noticed that above 60 Hz the damping estimates resulting from the input signals of $1/f^0$ and $1/f^1$ fall very close to the pure sine estimates. The estimates from $1/f^2$ in the same region are higher than the pure sine estimates. Below 60 Hz, none of the random signals shows a good agreement with the pure sine values. One other thing noted is the fact that the damping estimates from $1/f^0$and $1/f^1$ weighted random excitations are about the same throughout the entire frequency range. This observation holds true for the stiffness estimates as well. Just as with the damping estimates, the stiffness variations from $1/f^2$ weighting are higher than the other two, while the $1/f^0$ and $1/f^1$ weighted results are very close to one another. The results of stiffness for $1/f^0$ seem to mirror the pure sine values above 70 Hz and below 20 Hz. Between 20 and 70 Hz, the estimates are higher than the pure sine estimates. One noticeable result shown in the stiffness graphs is that the estimates resulting from $1/f^0$ and $1/f^1$, below 60 Hz, fall below zero which needs some explanation.

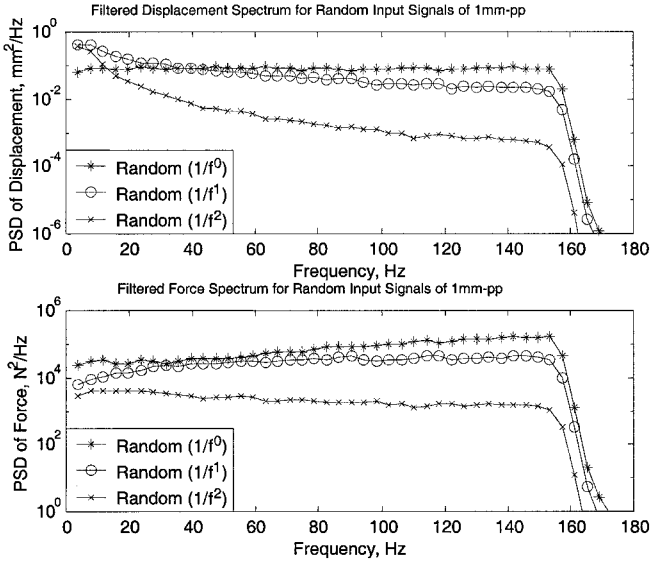


**Fig. 5** Power spectral densities of input displacement and output force for random input signals

It was found that the phase below 60 Hz rises above 90°. This results in the stiffness estimates in these areas being negative. In other words, $K = K^* \cos(\Phi)$, and the cosine function changes sign at 90°. It was hypothesized that the phase jumps were caused by the shock absorber being overdriven by the amount of energy input at the higher frequencies. This was speculated because the amplitude for random $1/f^0$ weighting is the same at all frequencies. It is known that this is not the case when the shock absorber is in operation. In order to test this hypothesis, the random input excitation of $1/f^0$ was filtered to contain only frequencies below 60 Hz. The shock absorber was then excited using this lower-frequency band limited random signal. As shown in Fig. 7, it was found that the phase angle between input displacement and output force of this abbreviated random signal does not contain any jumps in phase like the earlier broader frequency excitation.

As shown in Fig. 7, the stiffness estimates become more realistic for the abbreviated $1/f^0$ random signal as expected. The stiffness estimates from this filtered input signal fall close to the pure sine estimates. However, when examining the damping estimates in Fig. 7, the same observation does not hold true. The damping estimates obtained from the random signal, below 60 Hz, do not have the same estimates as obtained from the pure sine waves. The estimates from the abbreviated random signal have higher damping estimates than the pure sine estimates.

In summary, if the shock absorber is being driven by narrow-band random excitation, the estimations for both stiffness and damping agree somewhat with pure sine wave test data. However, there is no reason to assume that the pure sine excitation yields the best estimations because, in practice, shock absorbers experience broadband frequency inputs and their dynamic properties are generally non-linear. The classic force–velocity plots for this shock absorber for single-sine, sine-on-sine and random input excitations are shown in Figs 8a to c. The slope of the force–velocity plot is related to classical viscous damping. Although the shock absorber behaviour appears to be linear for a single-sine excitation, it is non-linear for the other two cases presented. It is,

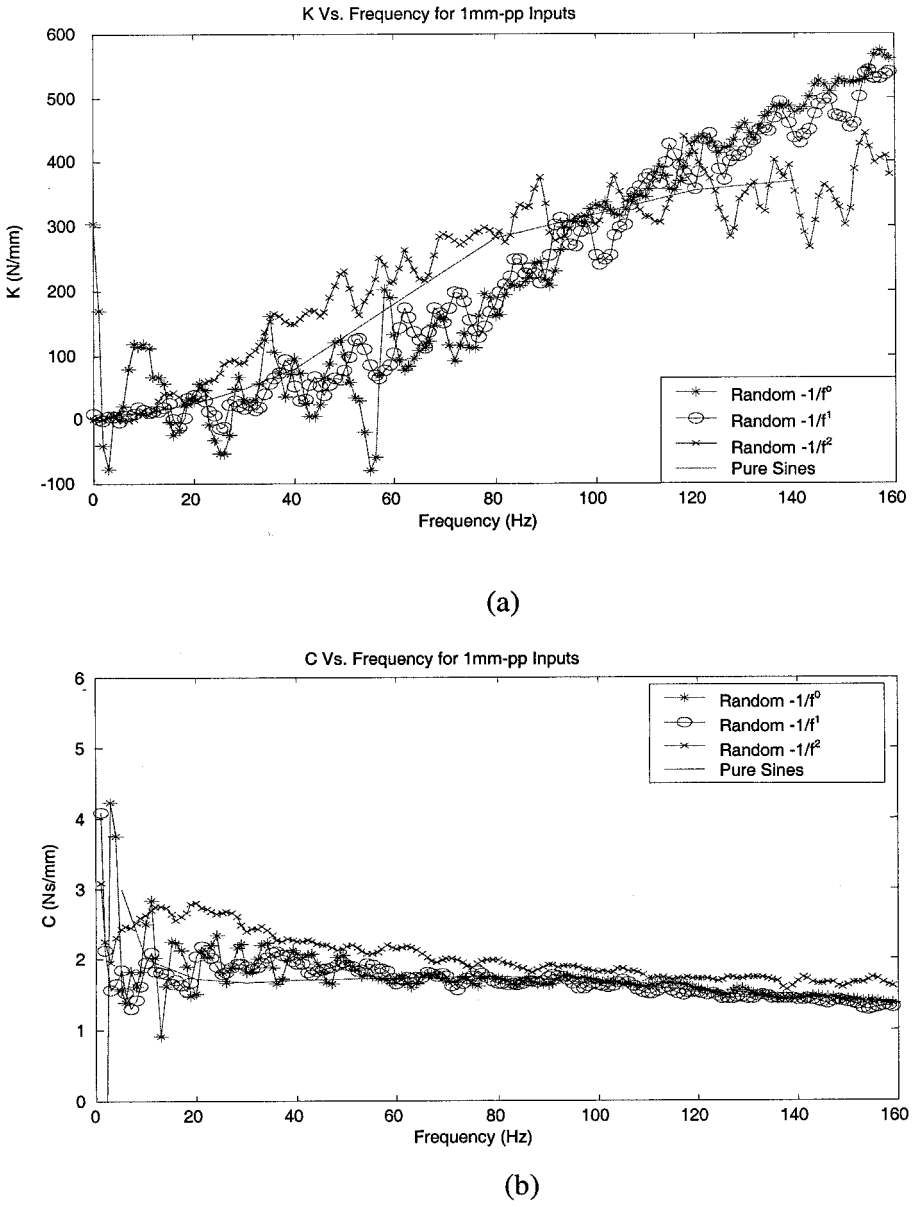


**Fig. 6** Damping and stiffness versus frequency for random input compared with pure sine wave input

however, possible to obtain equivalent linear damping from these plots using a least-squares curve fit.

## 5 ROAD EXCITATION

In an effort to obtain a true shock absorber response in operation, a mid-size sedan was instrumented with two 356 B08 PCB accelerometers. One accelerometer was positioned on the top of the shock and one positioned at the bottom of the shock. The automobile was then driven on a smooth highway, a semi-rough paved road and a rough dirt road, while the time traces of the accelerometers were recorded using the LMS Road Runner acquisition system. The difference between the two acceleration signals was integrated twice in the frequency domain, to obtain the input displacement. The signals were filtered below 2.5 Hz and above 160 Hz. The input displacement obtained from the rough road profile is shown in Fig. 9a.

The time trace shows a maximum displacement of about 14 mm. The frequency domain representation of the road profile is quite interesting. The maximum displacements are about 0.45 mm and occur around 5 Hz. The displacement inputs, above 80 Hz, are very low compared with the inputs at lower frequencies. Owing to limitations of the current hydraulic test machine, these higher-frequency, lower-amplitude signals are difficult to reproduce in a laboratory test. This results in a low confidence level in the parameters estimated above 80 Hz. Hence, the frequency spectrum from the road data was modified by adding a random phase to it. This yields a

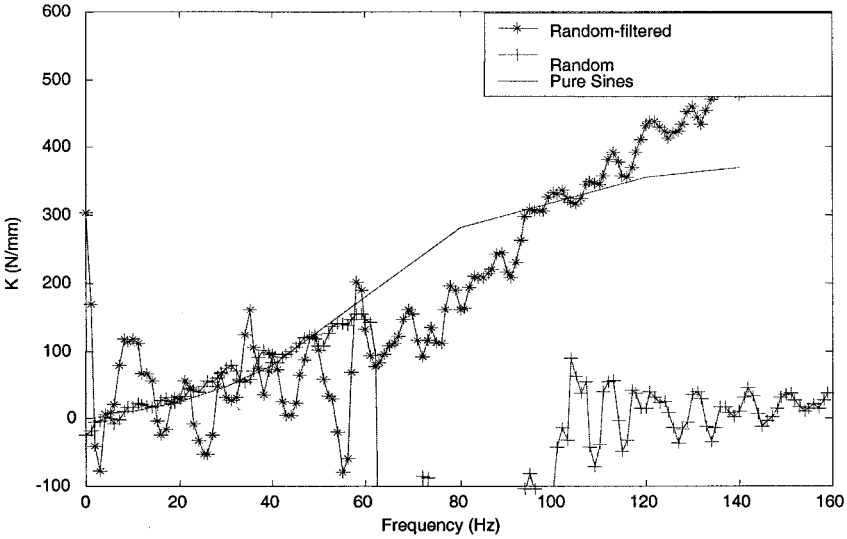


(a)

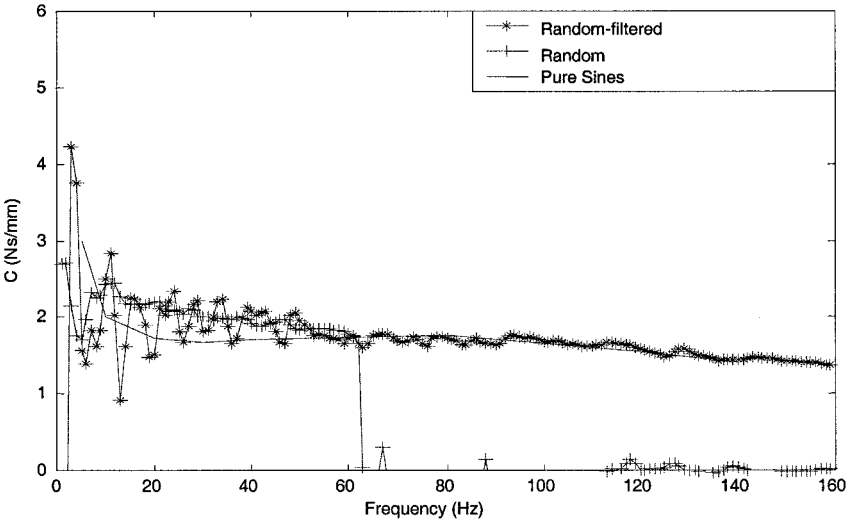


(b)

**Fig. 7** Comparison of damping and stiffness estimates for pure sine and random input

'shaped' random signal with the same frequency spectrum as the original road data. This is illustrated in Fig. 9b, where it is seen that the frequency spectrum is the same as for both the actual road response and the randomized road response. The time signal, however, is a random signal with the same spectral content as the measured road data.

Figure 10 shows the estimated parameter results from the shaped road frequency random excitation after curve fitting the results. It is seen that the stiffness and damping estimate are close to those of pure sine waves. In the case of stiffness, the estimates are slightly lower than those obtained with pure sine excitation. The smooth road stiffness estimations are well below the pure sine estimations from other road profiles. This is believed to be a result of poor reproduction of the small displacements seen on the smooth road in the laboratory. Therefore, this series should be disregarded since the data are approaching the noise floor of the measurement system. The two other road profiles are very close to one another and are believed to be meaningful. The damping estimates using the shaped road spectrum fall almost on top of the estimated damping from pure sine excitation. The stiffness and damping curves are much more realistic for an automotive shock absorber using this method as opposed to the pure road response excitation.

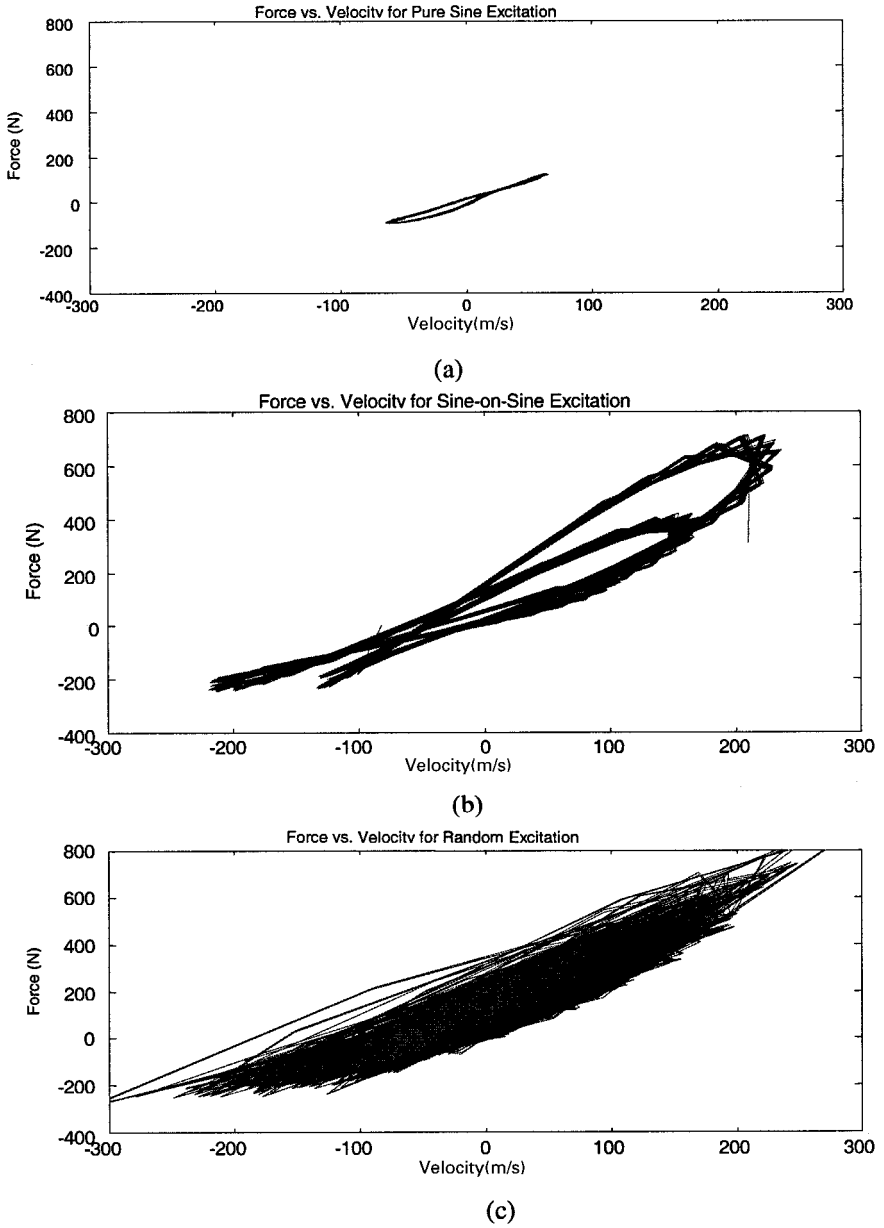


**Fig. 8** Force versus velocity plots of the shock absorber for different inputs

## 6 CONCLUSIONS

The results of this study have proven a number of things. Firstly, it is shown that, when two sine waves are added together and used to actuate a shock absorber, the parameters estimated at each frequency are dependent on one another. The dependence is a function of the frequency separation and relative amplitudes of the two waves. In the case where one frequency is higher than the other, the higher frequency maintains its parameters whereas the lower-frequency parameter estimations are very low. However, when random excitation in a narrow band was used, the parameters estimated were close to the estimations using pure sine waves.

It has been shown that all the estimated parameters can be found at once when using a shaped random signal. The best type of shaped random is one that has the same frequency spectrum to that experienced by the shock absorber in practice. When using this type of shaped random signal, the parameters estimated are close to the pure sine parameter estimations. The use of this type of realistic excitation has two advantages:

1. The actual test takes far less time than the stepped sine sweep.
2. Owing to the short test time, the effects of temperature on the estimated stiffness and damping are minimized since the temperature of the shock absorber does not change significantly during the test.

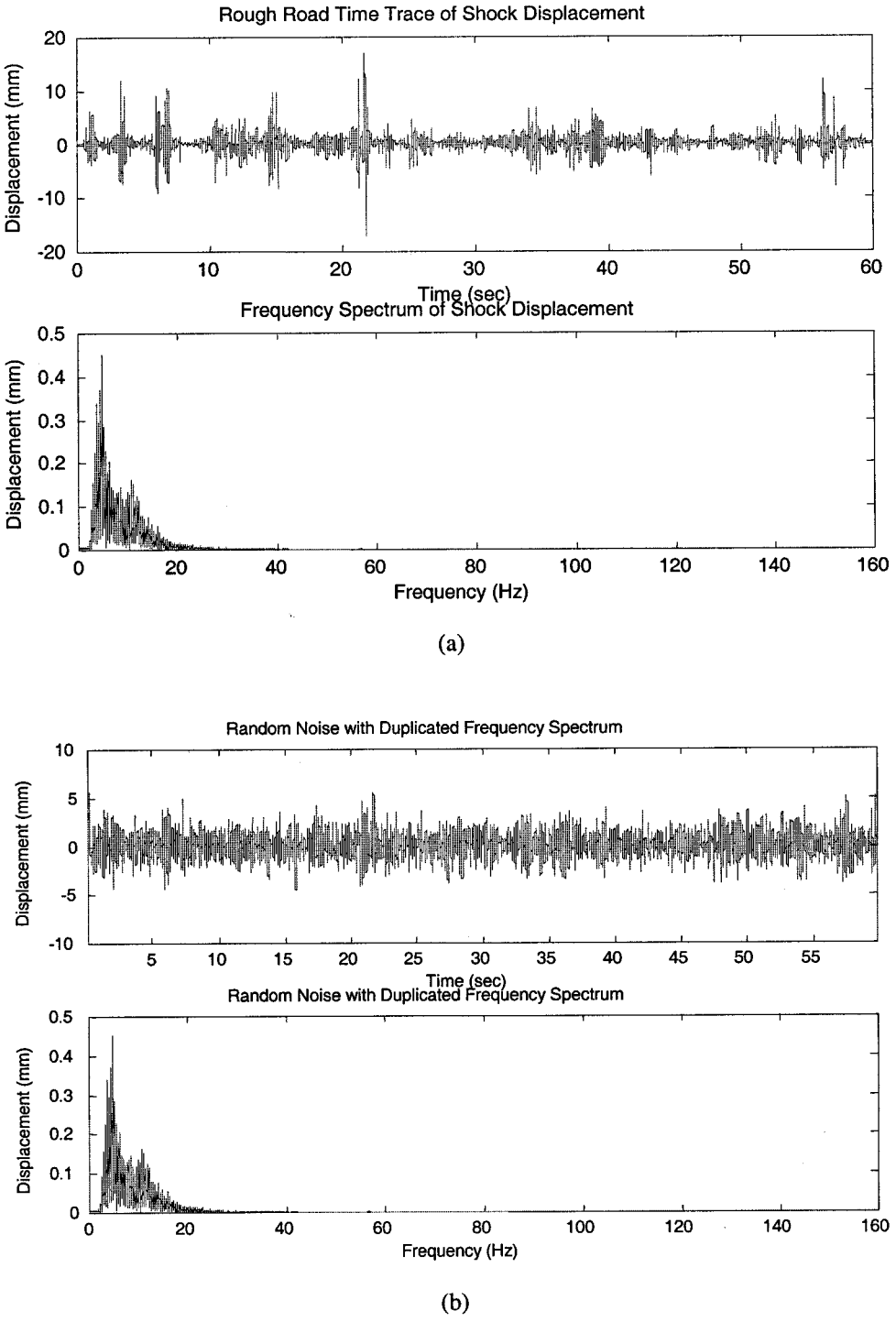


**Fig. 9** Actual road response and randomized road response in time and frequency axes

Finally, it will be useful to study the influence of different input excitation using a 'physical' model of a shock absorber. This would allow a designer to conduct parametric studies to evaluate the effects of design parameters on the dynamic performance of the shock absorber.

## ACKNOWLEDGEMENTS

This work was made possible through a University Research Program grant from Ford Motor Company. The authors would like to thank Dr David Griffiths of Ford Motor Company for his sponsorship and support.

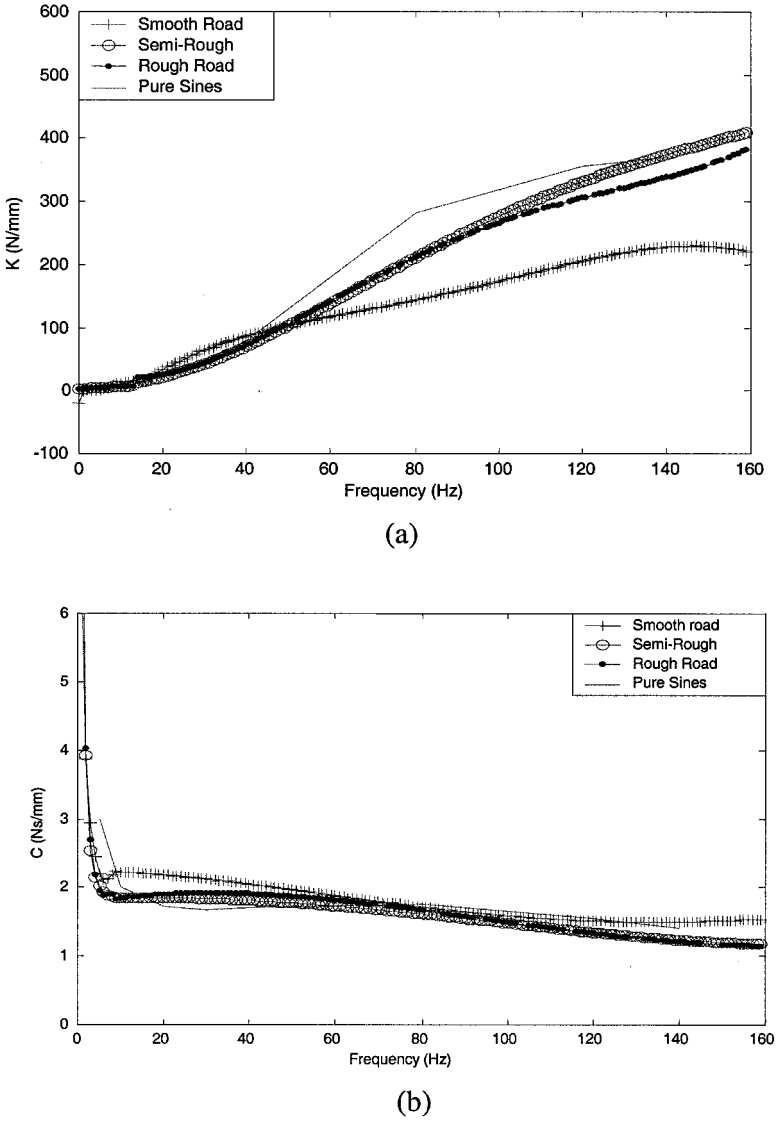


**Fig. 10** Damping and stiffness versus frequency from shaped random input

## REFERENCES


1 **Rao, M. D., Gruenberg, S.** and **Torab, H.** Measurement of dynamic properties of automotive shock absorbers for NVH. In Proceedings of SAE 1999 Noise and Vibrations Conference, Traverse City, 1999, pp. 1433–1438.

2 **Cafferty, S., Worden, K.** and **Tomlinson, G.** Characterization of automotive shock absorbers using random excitation. *Proc. Instn Mech. Engrs, Part D, Journal of Automobile Engineering*, 1995, **209**.

3 **Belingardi, G.** and **Campanile, P.** Improvement of the shock absorber dynamic simulation by the restoring force surface mapping method. In Proceedings of 15th International Seminar on *Modal Analysis and Structural Dynamics*, Leuven, Belgium, 1990, pp. 441–454.

4 **Duym, S., Schoukens, J.** and **Guillaume, P.** A local restoring force surface method. In Proceedings of 13th International Modal Analysis Conference, Nashville, Tennessee, 1995, pp. 1392–1399.

5 **Lang, H. H.** A study of the characteristics of automotive dampers at high stroke frequencies. PhD thesis, University of Michigan, 1977.

6 **Morman, K.** A model for the analysis and simulation of hydraulic shock absorber performance. Part I: theoretical development (SR-83-043); Part II: parameter identification and model validation studies (SR-86-61), Ford Motor Company Research Staff Reports.

7 **Reybrouck, K.** A non-linear parametric model of an automotive shock absorber. SAE paper 940869, Vehicle Suspension and System Advancements, SP-1031, 1994, pp. 79–86.